Development of hyaluronan-based dissolving microneedle arrays for dermal vaccination

Leone, M.

Chapter 4

Hyaluronan-based dissolving microneedles with high antigen content for intradermal vaccination: formulation, physicochemical characterization and immunogenicity assessment

Adapted from Eur J Pharm Biopharm 2019 (134):49-59

Mara Leone[1], Marjolein I. Priester[1], Stefan Romeijn[1], M. Reza Nejadnik[1], Juha Mönkäre[1], Conor O'Mahony[2], Wim Jiskoot[1], Gideon Kersten[1,3,*], Joke A. Bouwstra[1,*]

[1] Division of BioTherapeutics, Leiden Academic Centre for Drug Research (LACDR), Leiden University, Leiden, the Netherlands

[2] Tyndall National Institute, University College Cork, Cork, Ireland

[3] Institute for Translational Vaccinology (Intravacc), Bilthoven, the Netherlands

[*] These authors contributed equally.

ABSTRACT

The purpose of this study was to optimize the manufacturing of dissolving microneedles (dMNs) and to increase the antigen loading in dMNs to investigate the effect on their physicochemical properties. To achieve this, a novel single-array wells polydimethylsiloxane mold was designed, minimizing antigen wastage during fabrication and achieving homogeneous antigen distribution among the dMN arrays. Using this mold, hyaluronan (HA)-based dMNs were fabricated and tested for maximal ovalbumin (OVA) content. dMNs could be fabricated with an OVA:HA ratio as high as 1:1 (w/w), without compromising their properties such as shape and penetration into the *ex vivo* human skin, even after storage at high humidity and temperature. High antigen loading did not induce protein aggregation during dMN fabrication as demonstrated by complementary analytical methods. However, the dissolution rate in *ex vivo* human skin decreased with increasing antigen loading. About 2.7 µg OVA could be delivered in mice by using a single array with an OVA:HA ratio of 1:3 (w/w). Intradermal vaccination with dMNs induced an immune response similar as subcutaneous injection and faster than after hollow microneedle injection. In conclusion, results suggest that (i) the polydimethylsiloxane mold design has an impact on the manufacturing of dMNs, (ii) the increase in antigen loading in dMNs affects the microneedle dissolution and (iii) dMNs are a valid alternative for vaccine administration over conventional injection.

GRAPHICAL ABSTRACT

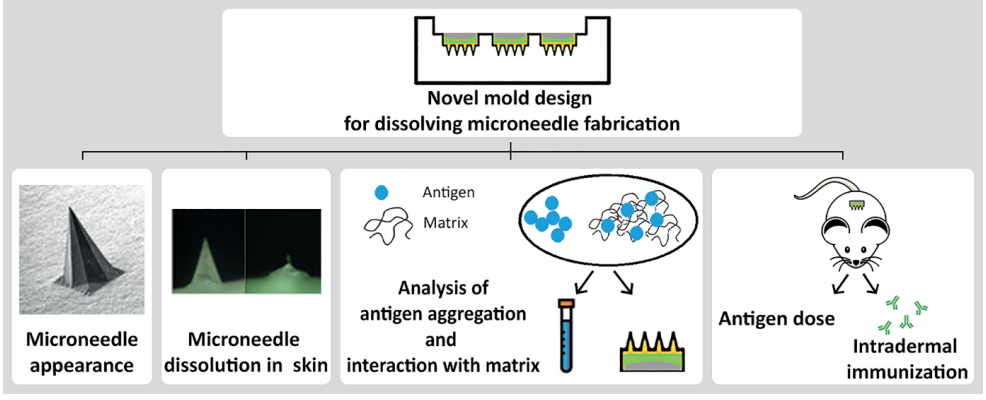

Keywords: dissolving microneedles, hyaluronan, antigen loading, antigen aggregation, vaccine delivery, skin immunization.

1. INTRODUCTION

The skin is an attractive target for vaccination since it is a very immune-competent organ. Several types of antigen presenting cells (APCs) such as Langerhans cells (LCs) and dermal dendritic cells (dDCs) are present in the skin [1,2]. They capture antigens and migrate to the draining lymph nodes for antigen-presentation to T-cells, evoking antigen-specific T-cell and B-cell activation. Pain-free delivery of antigen into the skin, however, is a challenge, but can be achieved by using microneedles. Microneedles (MNs) are microstructures (up to 1 mm in length [3]) capable to pierce the skin and deliver the antigen in the epidermis and dermis [3-7]. For pain-free delivery they should not reach the nerve endings in the skin [8]. Furthermore, immunization with MNs would not necessarily require healthcare personnel [4, 9-11].

Dissolving microneedles (dMNs) are a microneedle type consisting of fast-dissolving excipient, such as polymers or sugars, as matrix mixed with the active compound. They dissolve in the skin after insertion thereby releasing the active ingredient [3-7]. Several studies have demonstrated that vaccines delivered intradermally via dMNs can generate immune responses at least as strong as those generated by subcutaneous or intramuscular injections [11-16]. However, the advantages of dMNs include low cost of matrix materials [17] and avoidance of sharp needle wastage after immunization make dMNs an attractive delivery system for intradermal vaccination. Additionally, the dry state of dMNs in combination with stabilizing excipients can lead to vaccine thermostability [18].

Dissolving MNs are often fabricated by micromolding in which a polydimethylsiloxane (PDMS) mold is used to pour the vaccine/matrix formulation [13]. The PDMS mold design is crucial for an efficient and consistent fabrication, ideally leading to minimal loss of active material and a homogenous distribution of the antigen among the simultaneously produced microneedle arrays without antigen aggregation [19]. Furthermore, the mold design is important in determining the optimal matrix concentration for the dMN fabrication. Although different matrix materials have been tested and compared for the dMN fabrication [20,21], optimization of the formulation with respect to antigen loading and mechanical properties has to our knowledge not been reported. A more detailed analysis regarding the loading capacity of dMNs is relevant to encapsulate a sufficient amount of antigen to evoke an effective immune response. Furthermore, an increase in antigen concentration, besides drying steps during fabrication, may considerably compromise the protein stability as previously reported [19, 22-28]. The stability of protein in microneedle arrays has to be well determined, because presence of protein degradants such as aggregates may compromise safety and efficacy of the vaccine.

This study aimed to (i) reduce the antigen waste during dMN fabrication and achieve dose uniformity within a batch of arrays, (ii) maximize the antigen loading in dMNs while maintaining a sufficient dMN sharpness and stiffness to pierce human skin and minimizing antigen aggregation during fabrication, and iii) obtain dMNs that deliver a sufficient dose of

antigen in mouse skin *in vivo* to induce an immune response comparable with conventional injection. To this end, hyaluronan (HA) was used as matrix material for dMN fabrication and ovalbumin (OVA) was used as model antigen.

2. MATERIALS AND METHODS

2.1. Materials

Hyaluronan (HA) (sodium hyaluronate, average Mw 150 kDa) was purchased from Lifecore Biomedical (Chaska, MN, USA) and OVA (Grade V) was obtained from Sigma-Aldrich (St. Louis, MO, USA). Vinylpolysiloxanes A-silicone (Elite Double 32a Normal) and the two-component epoxy glue (Bison, Goes, The Netherlands) were obtained from The Zhermack Group (Badia Polesine, Italy) and Bison International B.V. (Goes, The Netherlands), respectively. Polydimethylsiloxane (PDMS, Sylgard 184) was obtained from Dow Corning (Midland, MI, USA). Solid silicon MNs, fabricated using a potassium hydroxide wet-etching process [29], were kindly provided by the Tyndall Institute (Cork, Ireland). PBS pH 7.4 for subcutaneous and hMN injections was obtained from B. Braun, Melsungen, Germany. Immunization studies and ELISA were performed by using endotoxin-free OVA (endotoxin level < 1 EU/mg) from Invivogen (Toulouse, France). 10 mM PB (7.7 mM Na_2HPO_4, 2.3 mM NaH_2PO_4, pH 7.4) was prepared in the laboratory.

2.2. Dissolving microneedles

2.2.1. Polydimethylsiloxane mold fabrication

The fabrication of dMNs by micromolding requires the use of a polydimethylsiloxane (PDMS) mold. The PDMS mold was fabricated by using a template of poly(methyl metacrylate) (PMMA). The PMMA template, made by milling on a HAAS VF1 VMC (Vertical Milling Machine, USA), presented nine square pedestals of 5.4 × 5.4 mm with a height of 2.5 mm. On top of each pedestal a single solid silicon microneedle array (16 MNs in 5.4 × 5.4 mm array, 300 µm length and 200 µm base diameter) was fixed (see Figure 1). Next, a PDMS solution consisting of a mixture of a silicone elastomer and curing agent, was prepared in a 10:1 ratio (w/w) following the manufacturer's instruction. The solution was mixed, degassed in a vacuum and subsequently poured on top of the PMMA template. Then the template was vacuumed and finally placed at 60 °C overnight to cure. The following day, the mold was carefully removed from the PMMA template (Figure 1).

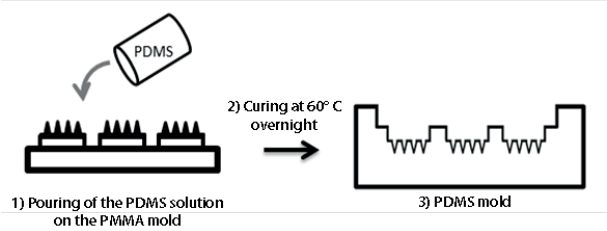

Figure 1. PDMS mold fabrication.

2.2.2. Preparation of dissolving microneedles

For the dMN preparation, the HA was dissolved in PB (10 mM, pH 7.4) and the solution was stored overnight to ensure the complete dissolution of HA. The next day, OVA in PB was added. Microneedle preparation was performed by pouring a selected OVA/HA solution in each well of the PDMS mold. Air bubbles were removed by vacuum cycles and to ensure complete filling of the micro-holes, the mold was placed in a centrifuge (1575 g, 37 °C, 3 h) (Beckman Coulter Allegra X-12R Indianapolis, IN, USA). Subsequently, additional OVA/HA solution was added to each well and steps of vacuum and centrifugation were repeated. Finally, the arrays were dried at 37 °C overnight.

To investigate the effect of the antigen loading in dMNs, a total of 12 OVA/HA compositions were used. These are provided in (Table 1).

Table 1. Overview of the different formulation compositions used to prepare the dMNs. In the Formulation approach A, the amount of HA was kept at 100 mg/ml while the amount of OVA varied. In the Formulation approach B, the amount of solids (OVA plus HA) was kept constant at 100 mg/ml but the ratio OVA/HA was changed. The control consisted of 10% HA. The compositions refer to the liquid formulations before dMN fabrication.

Composition	**Formulation approach A**				**Formulation approach B**							**Control**
OVA/HA (% w/v)	2.5/10	5/10	7/10	10/10	2.5/7.5	5/5	6/4	7/3	8/2	9/1	10/0	0/10
OVA (mg/ml)	25	50	70	100	25	50	60	70	80	90	100	0
HA (mg/ml)	100	100	100	100	75	50	40	30	20	10	0	100

After the overnight drying, an antigen-free bi-layered back-plate was prepared for all dMNs. A mixture of vinylpolysiloxane base and catalyst was prepared in a 1:1 ratio. The silicone solution was poured in each well and left curing for 20 min at room temperature (RT) to form the first layer of the back-plate. Next, a solution of two-components glue was placed

on top of the silicone layer. A sheet of solid PDMS and a 200 g weight were subsequently placed on top of the layers during the setting of the glue (2 h at 37 °C) to obtain a flat back-plate. Finally, the arrays were removed from the PDMS mold, and stored at RT in a desiccator until use.

2.3. Dissolving microneedle characterization

Microneedles were inspected by light microscopy (Stemi 2000-C, Carl Zeiss Microscopy GmbH, Göttingen, Germany) for shape, sharpness and for absence of empty cavities at the microneedle base after cutting tips transversely by using a stainless surgical blade (Swann-Morton, Sheffield, England). For high-resolution imaging, scanning electron microscopy (SEM, Nova NanoSEM-200, FEI, Hillsboro, OR, USA) was used. Prior to SEM imaging, the microneedle arrays were covered with a layer of 15 nm platinum/palladium (Sputter Coater 208HR, Cressington, Watford, UK). The instrument was operated at 5.00 kV and images were taken at magnifications between 300 and 600×.

2.4. Human skin

Human abdomen skin was obtained within 24 h after cosmetic surgery from local hospitals. After manual removal of the excess fat, the skin was stored at −80 °C until use. Before use, the skin was thawed in a humid petri dish at 37 °C for at least one hour and stretched with pins on parafilm-covered Styrofoam. The skin was cleaned with Milli-Q and 70% ethanol before the start of the experiment.

2.5. Microneedle penetration of *ex vivo* human skin

The arrays were applied by using an impact insertion applicator with a constant velocity of 0.54 m/s (Leiden University - applicator with uPRAX controller version 0.3) to ensure a reproducible piercing of dMNs [30]. After 18 s, the array was removed and 70 µl of 0.4% (w/v) trypan blue solution was applied on the penetration site for 1 h. After removal of the trypan blue solution with dry paper tissue, tape-stripping (approximately 10 strips) was performed (Avery 440 Gloss Transparent Removable, Avery Dennison) to remove the *stratum corneum* until the skin had a shiny appearance (Supplementary data, Figure S1). In this way only dMN penetration that reached the viable epidermis is taken into account [30]. Three arrays of each dMN composition were tested for their ability to penetrate *ex vivo* human skin from three different donors (i.e., n = 9 arrays for each dMN composition). The number of blue spots, indicating holes created by a microneedle, were counted for each individual array and divided by the total number of MNs on the array to obtain the penetration efficiency (PE) of each dMN composition (Equation 1) [30]:

$$\text{Penetration efficiency (\%)} = (\text{Number of blue spots}/16) \times 100\% \qquad \text{(Eqn. 1)}$$

2.6. Mechanical integrity of dissolving microneedles after storage

To examine the mechanical integrity after storage, three dMN arrays per each composition were exposed to different humidity and temperature in a desiccator as indicated in Table 2.

Table 2. Storage conditions of dMNs.

Storage period	Temperature (°Celsius)	Humidity (% Relative Humidity)
60 days	4	0
	Room temperature	0
	37	0
	60	0
4 hours	Room temperature	60
	Room temperature	82

To ensure 0% relative humidity (RH), microneedle arrays were stored over silica gel and to achieve 60 and 82 RH%, oversaturated salt solutions of sodium bromide and potassium chloride were used, respectively [31]. Prior arrays storage, the relative humidity was registered overnight every 20 min (Supplementary data, Figure S2) by using a data logger (EL-USB-2-LCD+, Lascar Electronics, Salisbury, UK) and a digital thermos-hygrometer (TFA-Fostmann GmbH & Co., Wertheim, Germany) to ensure constant humidity conditions in time. For each condition, five arrays per dMN composition were stored. After storage, two arrays were used for the visual characterization of dMNs and three arrays were used to investigate the capability of dMNs to pierce the *ex vivo* human skin as described in paragraph 2.6.

2.7. Microneedle dissolution in *ex vivo* human skin

Microneedles were pierced into the skin as described above and kept in the skin for 1 min, 5 min, 10 min or 20 min. Thereafter, arrays with remaining dMN tips were removed and stored in a desiccator until light microscopy analysis was carried out to determine the remaining microneedle tip length. Three arrays of each dMN composition were tested on three different skin donors for each time point (i.e., n = 3 arrays for each time point). The dissolved MN tip volume was calculated for each dMN composition (Supplementary data, Figure S3) and compared.

2.8. Analysis of protein stability

For the protein stability analysis, microneedle arrays (stored for less than one week in a desiccator RH 0% at room temperature) of all OVA/HA compositions (6 patches, one per composition) were dissolved overnight in PBS pH 7.4. Buffer volume was adjusted to obtain 0.5 mg/ml of OVA concentration.

2.8.1. Asymmetrical flow field-flow fractionation

In order to analyze the state of the antigen after microneedle dissolution, asymmetrical flow field-flow fractionation (AF4) was performed. The analysis was performed on all the compositions of OVA/HA both in solutions prior to microneedle fabrication and their corresponding microneedle arrays dissolved in PBS. Controls of OVA-only and HA-only, both in solution and as dissolved array, were also analyzed. AF4 measurements were performed on an Agilent 1200 system with a UV detector (280 nm) (Agilent Technologies, Palo Alto, California) combined with Wyatt Eclipse for AF4 separation and a multiangle laser light scattering (MALLS) detector (Wyatt Technology Europe GmbH, Dernbach, Germany). For the separation, a small channel equipped with a 350 µm spacer of medium width and a regenerated cellulose membrane with a cut-off of 10 kDa was used. The injection volume was 50 µl and the mobile phase was a solution of 50 mM of $NaNO_3$. In order to separate the aggregates in the samples (eluting later) from the monomer/dimers (eluting earlier), the samples were injected into the channel, followed by 1 min focus-flow. Thereafter, elution in the channel started with a cross-flow of 3 ml/min for 12 min. Then, after a total AF4 program time of 19 min, the cross-flow stopped to elute all remaining aggregates. The detector flow during elution was set to 1 ml/min. Calculation of the percentage of aggregates in the sample was done by calculating the area under the curve (AUC) of the aggregate peaks of the elugrams dividing by the total AUC of all peaks ('monomer and/or dimer' and 'aggregates') with Chemstation software from Agilent. The molecular weight of the species was calculated by relating the MALLS signal to UV according to the built-in functions in the Astra software version 5.3.2.22 (Wyatt Technology Europe GmbH, Dernbach, Germany).

2.8.2. Flow imaging microscopy analysis

A Micro-Flow Imaging (MFI) system (MFI5200, ProteinSimple, Santa Clara, USA), equipped with a silane coated flow cell (1.41 × 1.76 × 0.1 mm) and controlled by the MFI View System Software (MVSS) version 2, was used for flow imaging microscopy analysis. The system was flushed thoroughly with ultrapure water and PBS prior to each measurement to reduce the background counts of particles. After the rinsing step, the cleanliness of the field of view was checked visually. The background was zeroed by flowing PBS and performing the 'optimize illumination' procedure. Samples of 0.5 ml with a pre-run volume of 0.2 ml were analyzed at

a flow rate of 0.17 ml/min and a fixed camera rate of 22 flashes per second. The data recorded by the MVSS was analyzed with MFI View Analysis Suite (MVAS) version 1.2 after stuck particle removal procedure was performed by the software. The equivalent circular diameter (ECD), which is the diameter of a spherical particle that has an equivalent projection area as the particle imaged by MFI, was calculated as a measure of the particle size. The particle concentrations (particles/ml) were obtained and plotted in function of the particle size.

2.8.3. Nanoparticle tracking analysis

Nanoparticle tracking analysis (NTA) was performed at room temperature with a NanoSight LM20 (NanoSight Ltd., Amesbury, United Kingdom) equipped with a 640 nm laser and operating at an angle of 173° with respect to the flow cell (100 × 80 × 10 μm). Samples were injected into the chamber by an automatic pump (Harvard Apparatus, catalog no. 98–4362, Holliston, USA) using a sterile 1 ml syringe (BD Discardit II, New Jersey).

The following settings were used for tracking of the particles: background extract on; brightness 0; gain 1.00; blur size 3 × 3; detection threshold 10, viscosity equal to that of water. All other parameters were set to the automatic adjustment mode. For each sample a 90 s video was captured with shutter set at 1495 and gain at 680. The video was analyzed by using the NTA 2.0 Build 127 software.

2.9. Mice

Female BALB/c (H2d) (Charles River (Maastricht, The Netherlands), 8–11 weeks old at the beginning of the studies, were maintained under standardized conditions in the LACDR animal facility. The mice were randomly assigned to groups of 8 mice. Quantification and immunization studies were approved by the ethical committee on animal experiments of Leiden University (License number 14241).

2.10. Quantification of ovalbumin delivery in mouse skin *in vivo*

2.10.1. Preparation of infrared labeled ovalbumin

To quantify OVA release in mouse skin *in vivo*, OVA was labeled with an infrared dye (IRDye 800CW, LI-COR, Lincoln, Nebraska USA) (OVA-IR800) according to the manufacturer's instructions. The infrared signal of labeled OVA was measured by Tecan Infinite M1000 plate reader (Männedorf, Switzerland) at excitation and emission wavelengths of 774 nm and 789 nm, respectively.

2.10.2. Ovalbumin quantification

Based on the dissolution studies in *ex vivo* human skin, microneedle arrays of 2.5% OVA and 7.5% HA (n = 9) were selected for quantification of OVA in mouse skin *in vivo* and 5% of the total OVA was replaced with OVA-IR800.

The dMNs were inserted into anaesthetized female BALB/c (H2d) (Charles River (Maastricht, The Netherlands)) shaved flank skin for a period of 20 min after which the array was removed. Mice were euthanized and the near-infrared fluorescence of the delivered OVA-IR800 was measured in a Perkin-Elmer IVIS Lumina Series III *in vivo* imaging system (Waltham, MA, USA), by using a ICG bkg excitation filter and an ICG emission filter, acquisition time 4 s, F-stop 2, binning 4 and field of view of 12.5 cm. Perkin-Elmer Living Image software version 4.3.1.0 was used for image acquisition and analysis. Infrared data were processed using region of interest (ROI) analysis with background subtraction consisting of a control region of the skin.

To enable the quantification of the delivered amount of OVA-IR800, a calibration curve in *ex vivo* mouse skin was made by injecting different volumes of a formulation containing an OVA:HA ratio of 1:3 (w/w). Intradermal microinjections of OVA-IR800 were performed at OVA-IR800 doses between 62.5 and 1000 ng by using the in house fabricated hollow microneedle (hMN) injection system reported elsewhere [32-34].

2.11. Immunizations

To evaluate the functionality of dMNs as vaccination method, the dMNs with a composition of 2.5% OVA and 7.5% HA was chosen to perform immunization study. The immunization groups (n = 8) are reported in Table 3.

Table 3. Immunization study parameters.

Immunization route	Application method	Group name	OVA dose (µg)
Intradermal	Dissolving MNs	OVA/HA dMNs[a]	2.7
	Single hollow MN (10 µl, 120 µm injection depth)	OVA hMN	4.0
		OVA/HA hMN[b]	4.0
Subcutaneous	Conventional 26G needle (100 µl)	OVA sc	4.0
		PBS sc[c]	-

[a] 2.5% OVA/7.5% HA group as determined by OVA delivery from fluorescently labeled OVA-IR800 in mouse skin *in vivo*.

[b] 12 µg HA, resembling the OVA:HA ratio of dMNs group.

[c] PBS pH 7.4 (as negative control)

For single hollow microneedle injection and the dMN array application specially designed applicators were used as described previously [30, 32-34]. Immunizations were performed at day 1 (prime immunization), day 21 (boost immunization) and day 42 (2nd boost immunization). One day prior to the immunizations by dMN and hMN systems, the mice were shaved on the flank (approximately 4 cm^2). On the same day, venous blood (200 µl) was collected by tail vein incision in a 0.8 ml MiniCollect® tube. The blood was stored on ice before centrifugation (3000 g, room temperature, 10 min) to isolate serum, which was stored at −80 °C until analysis. Prior to vaccination, mice were anaesthetized by intraperitoneal injection of 150 mg/kg ketamine and 10 mg/kg xylazine. At day 63, all mice were bled by incision of abdominal/thoracic artery followed by scarification by cervical dislocation. Blood samples in 2.5 ml Vacuette® tubes were stored on ice before centrifugation at 1800 g (4 °C, 10 min) to isolate serum, which was stored at −80 °C until analysis.

2.12. Serum IgG assay

OVA-specific antibodies were determined by ELISA as described earlier [35]. OVA coated ELISA plate wells were blocked with bovine serum albumin (BSA) (Sigma-Aldrich, Zwijndrecht, the Netherlands) and subsequently, three-fold serial dilutions of serum were added to the plates and incubated for 1.5 h at 37 °C. The plates were incubated with horseradish peroxidase-conjugated goat antibodies against IgG total, IgG1 and IgG2a (Southern Biotech, Birmingham, AL, USA) for 1 h at 37 °C. 1-step TM ultra 3,3',5,5'-tetramethylbenzidine (TMB) (Thermo-Fischer Scientific, Waltham, USA) was used as substrate and the reaction was stopped with sulfuric acid (H2SO4) (95–98%) (JT Baker, Deventer, The Netherlands). The absorbance was measured at 450 nm on a Tecan Infinite M1000 plate reader (Männedorf, Switzerland) and the antibody titers were expressed as the log10 value of the mid-point dilution of a complete s-shaped absorbance-log dilution curve of the diluted serum level.

2.13. Statistical analysis

Microneedle penetration efficiency was analyzed by Kruskal–Wallis test with Dunn's multiple comparison test. Level of significance was set at $p < 0.05$. The remaining dMN length after dissolution at different time points was analyzed by two-way ANOVA with a Tukey's post-test ($p < 0.05$). IgG titers were analyzed using one-way ANOVA with Bonferroni post-test suitable in the software Prism (Graphpad, San Diego, USA). A p-value less than 0.001 was considered to be significant.

3. RESULTS

3.1. Polydimethylsiloxane mold optimization and dissolving microneedle fabrication

A novel PMMA template was designed so that in the PDMS mold each individual dMN array was fabricated in a separate well, referred to as single-array well design (Figure 2A). This has the advantage over our previously designed template resulting in multi-arrays well PDMS design [19] that (1) each well undergoes the same physical processing during the preparation of the dMN arrays, (2) dMN arrays of different compositions can be prepared in one fabrication process run and (3) the antigen loss could be reduced by pouring the matrix/antigen solution on each array-space (well), herewith avoiding to waste the solution on areas in between the wells. A comparison between the single-array well design and the multi-arrays well design is provided in Supplementary data, Figure S4.

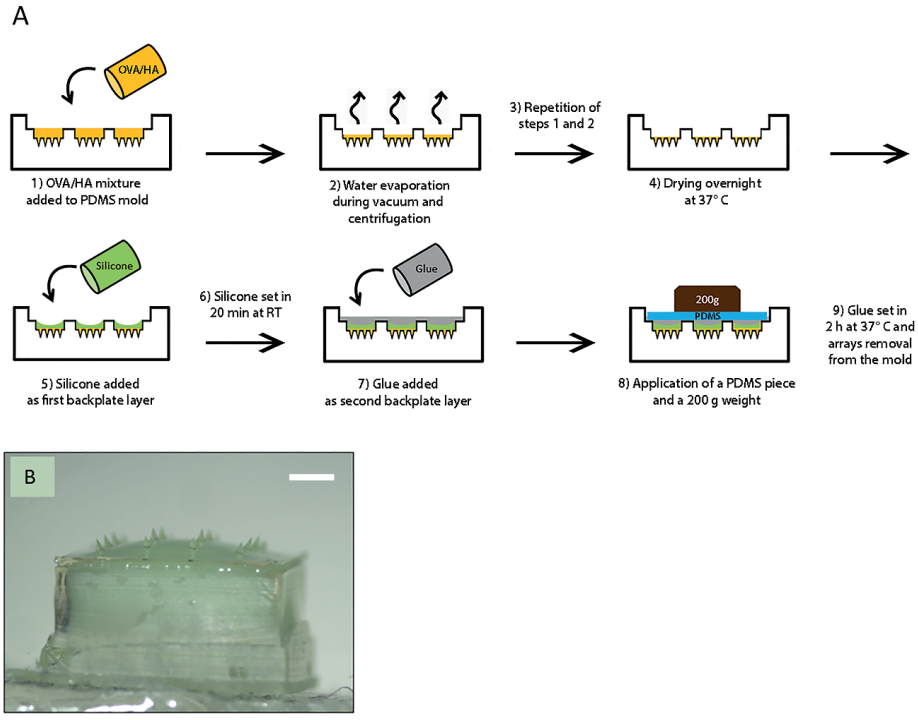

Figure 2. (A) Preparation scheme of dMNs and bi-layered back-plate using a single-array well mold. **(B)** Brightfield microscope images (1.25×) of a dissolving microneedle array with bi-layered back-plate (scale bar 1 mm). PDMS, Polydimethylsiloxane; RT, room temperature.

The single-array well PDMS design allowed the preparation of an antigen-free back-plate and thus less antigen is required for MN preparation. The antigen-free bi-layered back-plate consisted of a first layer of silicone and a second layer of glue (Figure 2A-B) and increases the easiness of MN array handling.

The PDMS mold was used to select the optimal HA concentration as control (Supplementary data, Figure S5) for the dMN fabrication. dMNs with HA concentration below 10% (w/v) in preparation mixture, showed empty cavities at the base of MN tip, whereas the use of concentrations of 10% (w/v) HA or above it resulted in dMNs without empty cavities at the base. The 10% HA concentration was selected as HA control because solutions with higher HA concentration were too viscous and thus difficult to handle. It was further observed that 10% (w/v) total solid content, i.e. reached by HA and OVA together content combined, could still give microneedles without empty cavities at the base (see Formulation approach B, Figure 3B).

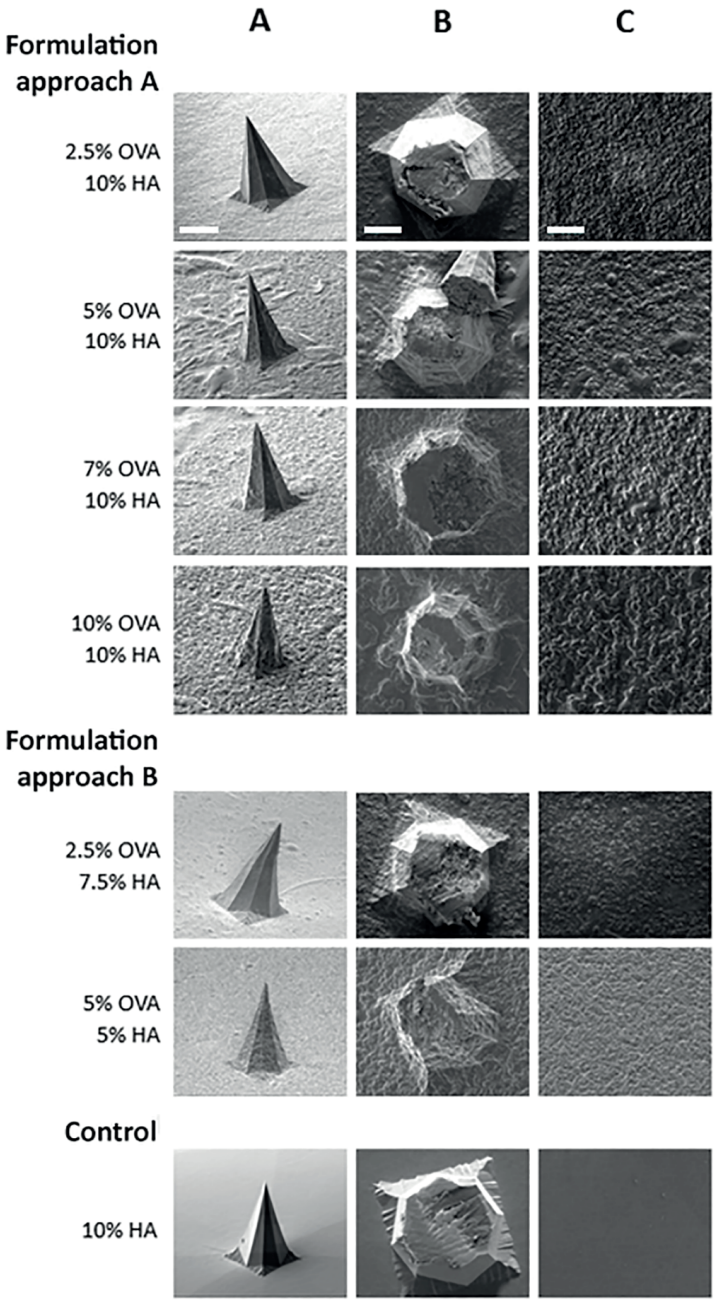

Figure 3. SEM images show increasing OVA concentration up to a weight ratio of 1:1 with HA allows the preparation of symmetrical and sharp dMNs. **(A)** dMNs lateral view (300×, scale bar 100 μm), **(B)** cut dMNs, upper view (600×, scale bar 50 μm) and **(C)** surface structure dMNs (600×, scale bar 50 μm).

3.2. Appearance of dissolving microneedles

To assess whether high antigen loading affects the quality of the dMNs, dMN arrays were prepared with increasing antigen content (Table 1). It was possible to increase the OVA content in the dMNs up to an OVA:HA ratio of 1:1 (w/w) (10% OVA/10% HA or 5% OVA/5% HA) without observing a decrease in the microneedle sharpness (Figure 3A). However, increasing the OVA content beyond 50% of total HA and OVA concentration led to inconsistencies in fabrication. The arrays were fragile, contained ruptures, and it was not possible to remove intact arrays from the PDMS mold (data not shown).

SEM (Figure 3B) and brightfield (data not shown) analysis of transversal-cut dMN showed no empty cavities in the inner side of MNs up to an OVA:HA ratio of 1:1 (w/w) in both approaches, indicating a homogeneous filling of the PDMS micro-holes during dMN fabrication.

For both Formulation approach A and B, changes in the surface structure in comparison with the HA only control were observed (Figure 3C). Increasing OVA content in dMNs increased the surface roughness in comparison with the control (10% HA), which had a smooth surface. However, this did not affect the sharpness and shape of dMNs.

3.3. Penetration ability of microneedle arrays into *ex vivo* human skin

To investigate whether differences in dMN composition affect the dMN penetration of the skin, the arrays were applied onto *ex vivo* human skin. Regardless of the composition, all dMNs penetrated the skin, with a penetration efficiency of almost 100% for all the compositions (Table 4).

Table 4. Penetration efficiency of dMN with different compositions. All data are presented as mean ± SD (n = 9). No significant difference ($p > 0.05$) was found by Kruskall–Wallis test with Dunn's multiple comparison test.

Sample	Penetration efficiency (%)
2.5% OVA/10% HA	99.3 ± 2.1
5% OVA/10% HA	100.0 ± 0.0
7% OVA/10% HA	100.0 ± 0.0
10% OVA/10% HA	98.6 ± 2.7
2.5% OVA/7.5% HA	100.0 ± 0.0
5% OVA/5% HA	96.8 ± 4.7
10% HA	99.3 ± 2.1

3.4. Mechanical integrity of dissolving microneedles after storage

As dMN arrays may be exposed to various temperature and humidity conditions during shipment, storage and administration, the effect of these conditions was investigated. Microscope analysis showed that storage at different temperature and humidity conditions (Table 2) did not affect the sharpness of the dMNs (data not shown). Furthermore, the storage conditions did not alter the skin penetration efficiency of the dMNs, which remained close to 100% for all dMN compositions and storage conditions (Table 5).

Table 5. Penetration efficiency of dMNs after storage. dMNs were stored (n = 3 per dMN composition) under the conditions indicated. All data are presented as mean ± SD. No significant difference ($p > 0.05$) was found by Kruskal–Wallis test with Dunn's multiple comparison test.

	4°C 0% RH	RT 0% RH	37°C 0% RH	60°C 0% RH	RT 60% RH	RT 82% RH
SAMPLE	**60 days**				**4 hours**	
Formulation approach A						
10% OVA/10% HA	100 ± 0.0	100 ± 0.0	87.5 ± 16.5	100 ± 0.0	97.9 ± 3.6	97.9 ± 3.6
2.5% OVA/10% HA	100 ± 0.0	100 ± 0.0	100 ± 0.0	100 ± 0.0	97.9 ± 3.6	100 ± 0.0
Formulation approach B						
2.5% OVA/7.5% HA	100 ± 0.0	100 ± 0.0	100 ± 0.0	100 ± 0.0	97.9 ± 3.6	100 ± 0.0
5% OVA/5% HA	97.9 ± 3.6	100 ± 0.0	97.9 ± 3.6	100 ± 0.0	91.7 ± 3.6	97.9 ± 3.6
Control						
10% HA	100 ± 0.0	100 ± 0.0	95.8 ± 7.2	97.9 ± 3.6	97.9 ± 3.6	95.8 ± 7.2

RH, Relative humidity; RT, Room temperature.

3.5. Microneedle dissolution in *ex vivo* human skin

Analysis of the dissolved MN volume percentage after an application of 1, 5, 10 or 20 min showed that the dissolution rate depends on the dMN composition.

All dMN compositions showed a gradual dissolution as a function of time (Figure 4A). For compositions with an OVA concentration in the liquid starting formulation higher than 2.5% (w/v) as 5% OVA/5% HA, 5% OVA/10% HA, 7% OVA/10% HA and 10% OVA/10% HA, a comparable dissolution rate was reached after 1, 5, 10 and 20 min respectively (Figure 4B). The leftover was still high in comparison with that of the control (10% HA) (Figure 4A).

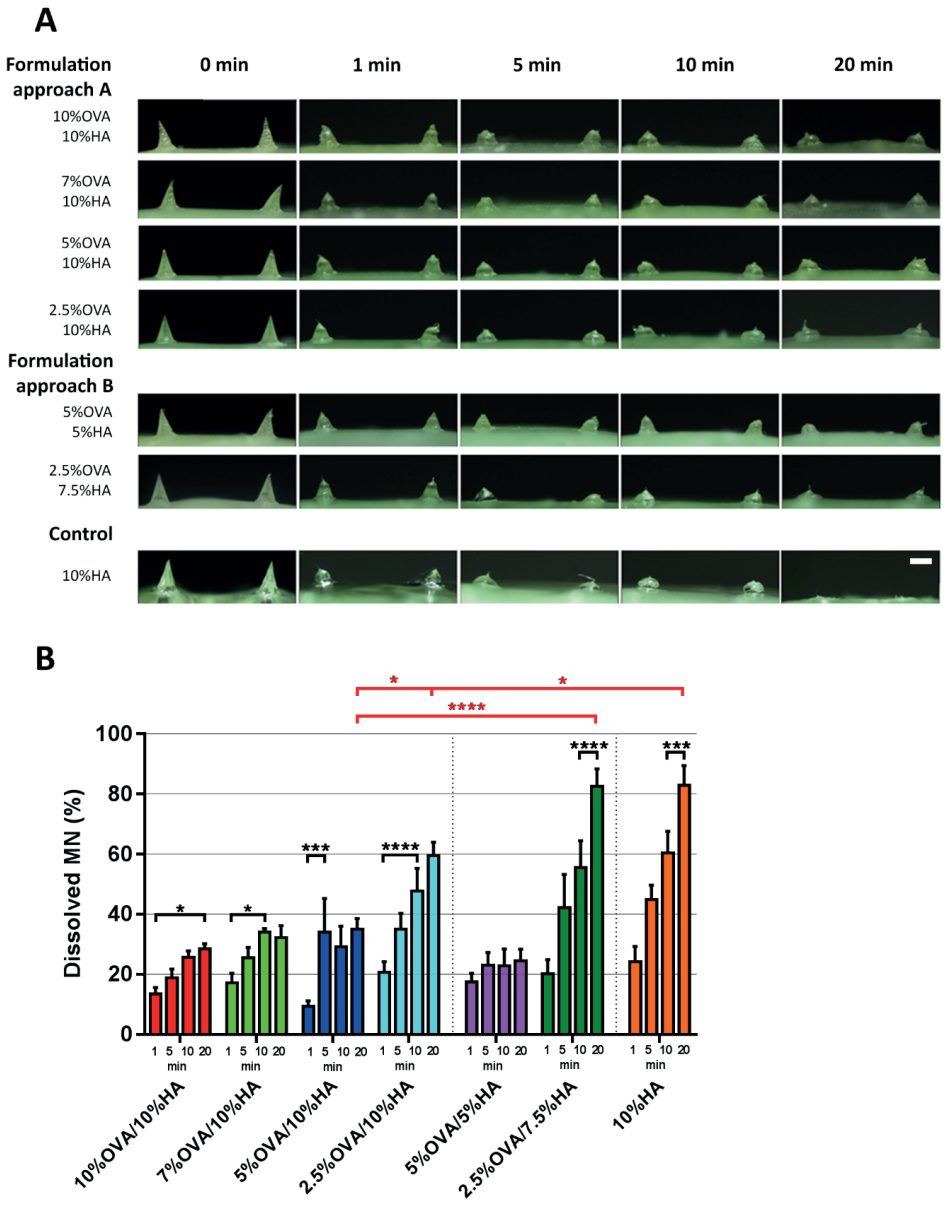

Figure 4. dMN dissolution in *ex vivo* human skin. **(A)** Representative light microscope images of dMNs before dissolution (0 min) and after 1, 5, 10 and 20 min dissolution in *ex vivo* human skin (40×). Scale bar is 200 µm; **(B)** Effect of time (1, 5, 10 and 20 min) on dissolution (statistics in black), showed per each dMN composition. Effect of formulation on dissolution (red statistics). Significance (*$p < 0.05$, ***$p < 0.001$ and ****$p < 0.0001$) was determined by a two-way ANOVA with a Tukey's post-test ($n = 3$). All data are presented as mean ± SEM.

The 2.5 %OVA/7.5% HA dMNs dissolved almost completely within 20 min after application, similarly to the control (Figure 4A and B). Although prepared with an equal OVA concentration in the liquid starting formulation as the 2.5% OVA/7.5% HA dMNs, the 2.5% OVA/10% HA dMNs reached maximal dissolution rate after 10 min resulting statistically different from the control (Figure 4B). As the 2.5% OVA/7.5% HA dMNs dissolved nearly completely after 20 min, we selected this composition for further studies.

3.6. Protein stability

The dMN fabrication conditions are mild, e.g., high temperature and extreme pH conditions are avoided, making chemical degradation unlikely to occur. Nevertheless, the antigen may encounter stress during the dMN preparation. The drying at high antigen concentrations may cause aggregation. To investigate whether submicron aggregates were formed during the dMN fabrication, AF4 analysis was performed. Figure 5A presents the UV elugrams of an OVA standard solution, a solution of 2.5% OVA/7.5% HA prior to dMN fabrication, and the same composition after dMN manufacturing and dissolving the MN array in PBS. Figure 5A shows how the OVA monomer eluted at 11.5 min, the OVA dimer eluted at 13.0 min and a small peak eluted after stopping the cross-flow at 19 min, indicating that OVA standard solution contained a minor fraction of aggregates with an average molecular weight of 2820 kDa calculated by MALLS detection. The 2.5% OVA/7.5% HA dissolved MN solution eluted at 12.1 min with a broader peak than OVA standard solution, indicating that OVA interacts with HA. However, the 2.5% OVA/7.5% HA starting solution showed a considerably broader peak (11.0–19.0 min), suggesting an even stronger interaction between OVA and HA. Furthermore, the peak of 2.5% OVA/7.5% HA solution after cross-flow stopping at 19.0 min indicates that the aggregate content and/or complexes between OVA and HA were considerably higher as compared to the 2.5% OVA/7.5% HA dissolved MN solution. All other compositions showed the same trend as the shown composition (data not shown). The dissolved HA-free dMNs, comprising only OVA (10% OVA w/v), showed an identical UV elugram as the OVA standard solution (results not shown), demonstrating that the drying/reconstitution process had no impact on the monomer/dimer content of plain OVA without HA present. Altogether, these results indicate a clear transient and reversible interaction between OVA and HA in solution, causing delayed elution of OVA both for OVA/HA solution prior to dMN fabrication and to a lesser extent for the corresponding dissolved MN array.

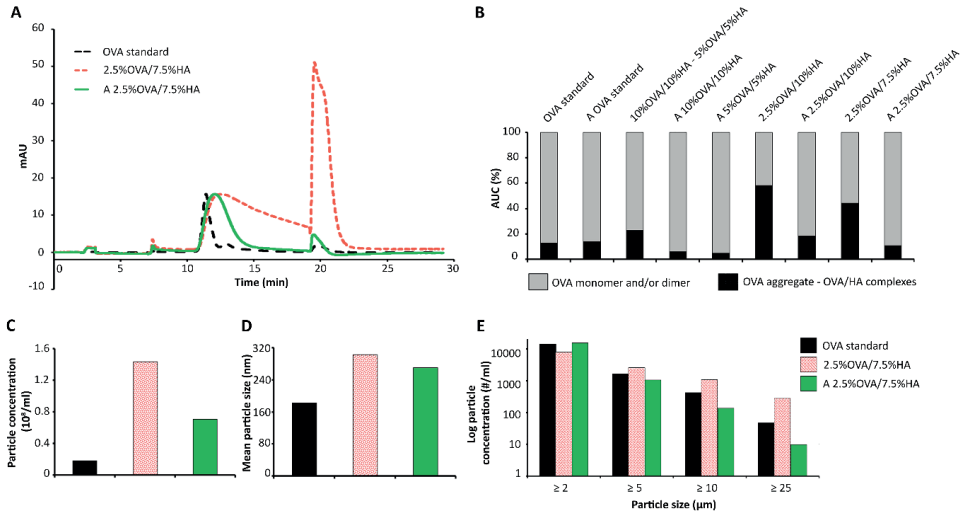

Figure 5. Protein aggregation analysis by AF4, NTA and MFI. **(A)** AF4 UV-based (280 nm) elugrams, normalized for the OVA standard solution peak at 11.5 min, of OVA standard solution (OVA standard, dark dashed line), 2.5% OVA/7.5% HA composition in solution prior to dMN fabrication (2.5%OVA/7.5%HA, light red dotted line) and its associated array dissolved in PBS (A 2.5%OVA/7.5%HA, green solid line); **(B)** Relative amount of OVA in aggregated and/or OVA/HA complexes (dark bars) and monomer and/or dimer state (light bars) calculated from the area under the curve of the AF4 UV elugrams for all OVA/HA compositions and OVA standard control; **(C–D)** Results of NTA of particle concentration and mean particle size, respectively, for the composition 2.5% OVA/7.5% HA both in solution prior to fabrication of dMNs and after array dissolution in PBS (A 2.5% OVA/7.5% HA); **(E)** Results of MFI shown as cumulative particle concentration vs particle size for the composition 2.5% OVA/7.5% HA before and after dMN fabrication. A, array.

The relative peak areas of monomer and/or dimer and aggregates expressed as percentages for each sample are shown in Figure 5B. It is evident that OVA/HA starting material contains more aggregates as compared to dissolved arrays for all compositions. Furthermore, the lower the OVA:HA ratio, in both solution and dissolved MN, the more OVA aggregates and/or OVA/HA complexes are found (see Figure 5B), again indicating an interaction of HA with OVA.

To rule out any particle formation that might have been missed during AF4 analysis, NTA and MFI analyses were performed for all compositions to monitor the presence of larger, nano- and micron-size aggregates, respectively. NTA showed that nanoparticle concentrations and particle sizes (Figure 5C and D, respectively, all other compositions showed similar trend (data not shown)) in the solutions of the dissolved arrays were lower than in the solutions prior to preparation of dMNs, corroborating the AF4 results. MFI analysis pointed in the same direction, i.e., it showed a lower micronsize particle content for all size ranges for the dissolved array compositions as compared to the freshly prepared OVA/HA mixtures and

even OVA standard solution (Figure 5E, all other compositions showed similar trend (data not shown)).

3.7. *In vivo* studies

As information on the delivered dose in the skin is crucial for designing immunization studies, the amount of OVA delivered into mouse skin *in vivo* after dMN array application was determined by using infrared labeled OVA. The dMN array with a composition of 2.5 %OVA/7.5% HA, that was selected for its optimal dissolution capability, was shown to deliver dose of 2.7 ± 1.3 µg (mean ± SD, n = 9) of OVA per array. The corresponding dissolved MN volume was of 76.4 ± 4.1% (mean ± SD, n = 9).

In order to investigate the immunogenicity of OVA delivered by dMNs in comparison with conventional subcutaneous injection, mice were immunized with OVA-dMNs (2.5% OVA/7.5% HA). As control, OVA (4 µg) was administered subcutaneously. In addition, hollow MNs were used to inject an exact dose of OVA with or without HA to investigate whether HA affects the immune response.

As shown in Figure 6, OVA administered via dMNs was equally immunogenic as subcutaneously injected OVA after both the prime and the two booster immunizations. For both groups, the first booster resulted in an overall increase in IgG total titers of about 2 log scales, whereas the second booster did not have a substantial additional effect on the total IgG titers. Interestingly, the IgG total responses were initially higher in the dMN group as compared to the mice receiving intradermally administered OVA with one hollow MN (OVA and OVA/HA). Only after the first or the second boost the IgG total titers of the hMN group OVA/HA and hMN group OVA respectively reached a comparable level as the dMN and s.c. groups. The presence of HA did not seem to have a major effect on the IgG total levels. The concentrations of OVA-specific IgG1 resembled closely the IgG total titers after each immunization point and IgG2a titers were absent (Supplementary data, Figure S6).

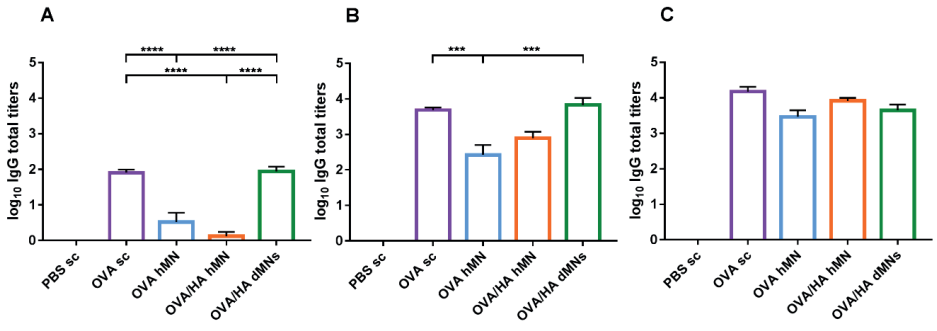

Figure 6. OVA-specific IgG antibody responses after vaccination. Mice were vaccinated either intradermally using dMNs (OVA/HA dMNs), hollow microneedle without HA (OVA hMN) and hollow microneedle with HA (OVA/HA hMN) or subcutaneously (OVA sc and PBS sc). Sera collected from the mice were assayed for OVA-specific IgG total titers after prime **(A)**, 1st boost **(B)** and 2nd boost **(C)**. Results are shown as mean ± SEM and statistical significance was determined by a one-way ANOVA with a Bonferroni post-test (***$p < 0.001$ and ****$p < 0.0001$).

4. DISCUSSION

The design of the PDMS mold plays an important role in the fabrication of dMNs. An optimization of the design by creating single-array well in the PDMS mold may have several advantages, such as a reduction in antigen waste during fabrication and an avoidance of heterogeneous distribution of the antigen content among the arrays of the single mold. It has been shown that the distribution of the protein within arrays prepared with a multi-arrays well design of a mold was not equal, most probably due to centrifugation forces in preparing the microneedle arrays [19]. In addition, this novel single-array well design allowed to work with different formulations during the same manufacturing run and to fabricate an antigen-free back-plate easy to handle. In the multi-arrays well PDMS mold the fabrication of an antigen-free back-plate for each single array was not possible because no single isolated arrays were prepared during manufacturing. The single-array well mold design was used in preliminary studies to identify the optimal HA concentration for a fabrication of cavity-free dMNs. Introducing an empty cavity at the microneedle base has been considered as a strategy to improve the delivery efficiency reducing the drug remaining in the microneedle after dissolution [36]. However, the size of the cavity is difficult to control, potentially leading to non-homogeneous dosing and reduced and variable needle strength. In our present study the optimal matrix concentration for cavity-free dMNs was 10% HA (w/v), while in a previous study using the multi-arrays well design mold and the same polymer, the arrays were fabricated by using lower HA concentrations [19]. This illustrates that for each mold design the polymer concentration should be optimized.

It was examined whether high protein antigen concentrations can be used in this novel way of producing the microneedles. A sufficient antigen dose is often required for achieving the desired effect and limited dose is one of main challenges of dMNs. It was observed that increasing the OVA content beyond 50% of total HA and OVA concentration led to fragile arrays. This may be related to a lack sufficient HA, which is needed for the structure of the microneedles provided by the polysaccharide hyaluronan network. Importantly, an increase in antigen content with a OVA:HA ratio from 1:4 up to a 1:1 (w/w) resulted in sharp dMNs that could efficiently penetrate the *ex vivo* human skin in a reproducible way. The penetration efficiency of almost 100% for all the compositions, enabled by the curved surface of the array and the presence of a back-plate [37], was comparable to that obtained in a previous study with silicon MNs applied via the same applicator [30].

Although the protein stability in dMNs is of critical importance, studies addressing this issue are scarce and they focus mainly on obtaining an immune response after dMN application to show preserved functionality after fabrication [13]. This, however, is an indirect and inaccurate way of monitoring antigen stability, as the immunogenicity of degraded antigens as well as antigen dose-response relationships are usually unknown. In this study, it was shown that the presented dMN fabrication method induced limited aggregation, even at very high OVA loading. This indicates that the conditions used during the micromolding were mild, as opposed to other fabrication methods [38, 39]. However, whether the same protein stability can be preserved for antigens different than OVA should be investigated. Remarkably, after dMN fabrication there was less aggregated OVA than in the OVA/HA solution used to produce the dMNs. This was observed for all OVA/HA solutions tested. Furthermore, AF4 showed a slight shift in elution time of OVA in the presence of HA, indicating some interaction between OVA and HA. This is in line with our previous study in which we showed reversible association between IgG and HA to occur [19]. The reason that this interaction was stronger in the solution before drying compared to dissolved needles may be caused by the fact that the needles were dissolved in PBS, resulting in increased ionic strength and, as consequence, in less electrostatic interactions between OVA and HA.

One important limitation that was encountered with a high OVA content (>2.5% (w/v)) in the arrays was a slower and reduced dMN dissolution in the skin. Increasing the hydrophilic polymer fraction did not avoid this, suggesting that the total OVA/HA concentration in the solution prior fabrication is affecting the dissolution of microneedles. However, when the selected 2.5% OVA/7.5% HA dMNs were used, the dissolution rate of dMNs was reasonably high. Moreover, the dissolved MN volume reached after application for 20 min in mouse skin *in vivo* (76.4 ± 4.1%) and in *ex vivo* human skin (82.6 ± 14.2%) were equal, proving a similar dissolution of dMNs in two different skin types. Interestingly, our studies demonstrate a faster dissolution of the control (10% HA) and 2.5% OVA/7.5% HA dMNs in comparison with HA dMNs reported in literature, such as 60 min and 120 min for complete dissolution of 300 µm and 800 µm length dMNs respectively [14, 40, 41]. This difference in dissolution time might be explained by differences in preparation conditions, although in some papers these

are not specified in detail. Also, the molecular weight of the HA used may be different. Other variables affecting dissolution time are the presence of excipients in dMNs [40], the type and quality of the skin used for dMN application (e.g., mice [14, 40] or rats [14, 41]), the use of an applicator, applicator settings and the experimental details of dissolution studies (*ex vivo* or *in vivo*).

Importantly, storage at different temperature or humidity values did not affect the dMN integrity. Contrasting results were reported by Hiraishi et al., who showed that high humidity caused dMN bending during use which prevented skin piercing [40]. However, in that case longer conical dMNs (800 μm) were tested and the MN design may play a role resulting the tetrahedral design of dMNs from the present study stronger [15, 42].

Prior to the immunization studies, the dose of OVA delivered in mouse skin *in vivo* from the selected 2.5% OVA/7.5% HA dMNs was quantified and estimated to be approximately 3 μg. This dose is in the range of a human dose of some licensed vaccines. Functionality of dMNs and retention of OVA after fabrication were proved through *in vivo* studies, showing comparable immunogenicity between dMNs and subcutaneous groups. Furthermore, the role of the HA as immunomodulator was investigated because of contrasting results in the literature [43-48]. The presence of HA with a mean molecular weight of 150 kDa did not affect the immune response, suggesting its inert nature as matrix material.

Finally, the higher response in the dMNs group than in the OVA hMN group after prime and first boost immunizations indicate that OVA administration by dMNs results in a faster response than administration by hMN. This may be due to a slower release of the antigen into the skin from dMNs than from hMN due to the dissolution step. Moreover, the different numbers of needles penetrating the skin may play a role: a hollow MN delivers the antigen as a small bolus at one site, whereas the dMNs deposit 16 small doses over a larger area. The slower release together with the broader antigen distribution and a potentially higher tissue damage and cell death [13, 49] from dMNs may result in a faster and higher response. The lack of IgG2a response was expected as no adjuvant was added to the MN formulation [50]. This may be subject of a follow-up study.

5. CONCLUSIONS

In summary, our study demonstrates that the design of the PDMS mold is a critical parameter in the fabrication of dMNs and that high antigen content in HA-based dMNs does not affect the sharpness and capability to pierce the skin of dMNs. dMNs can be manufactured with ovalbumin:hyaluronan ratio as high as 1:1 (w/w) without aggregate formation. However, the higher the antigen loading the lower is the dissolution rate of dMNs in the skin. Finally, vaccination by means of dMNs was shown to evoke a comparable response as by conventional subcutaneous injection and a faster response than hMN injection, illustrating the potential of dMNs for intradermal vaccine delivery.

Conflict of interest

Wim Jiskoot is a scientific advisor at Coriolis Pharma, Martinsried, Germany.

REFERENCES

1. L. Engelke, G. Winter, S. Hook, J. Engert, Recent insights into cutaneous immunization: how to vaccinate via the skin, Vaccine, 33 (2015), pp. 4663-4674
2. M. Kaurav, S. Minz, K. Sahu, M. Kumar, J. Madan, R.S. Pandey, Nanoparticulate mediated transcutaneous immunization: myth or reality, Nanomedicine, 12 (2016), pp. 1063-1081
3. K. van der Maaden, W. Jiskoot, J. Bouwstra, Microneedle technologies for (trans)dermal drug and vaccine delivery, J. Control Release, 161 (2012), pp. 645-655
4. K. Ita, Transdermal delivery of drugs with microneedles: Strategies and outcomes, J. Drug Deliv. Sci. Tec., 29 (2015), pp. 16-23
5. S. Indermun, R. Luttge, Y.E. Choonara, P. Kumar, L.C. du Toit, G. Modi, V. Pillay, Current advances in the fabrication of microneedles for transdermal delivery, J. Control Release, 185 (2014), pp. 130-138
6. E. Larraneta, M.T.C. McCrudden, A.J. Courtenay, R.F. Donnelly, Microneedles: a new frontier in nanomedicine delivery, Pharm. Res.-Dordr., 33 (2016), pp. 1055-1073
7. T.M. Tuan-Mahmood, M.T.C. McCrudden, B.M. Torrisi, E. McAlister, M.J. Garland, T.R.R. Singh, R.F. Donnelly, Microneedles for intradermal and transdermal drug delivery, Eur. J. Pharm. Sci., 50 (2013), pp. 623-637
8. N.R. Hegde, S.V. Kaveri, J. Bayry, Recent advances in the administration of vaccines for infectious diseases: microneedles as painless delivery devices for mass vaccination, Drug Discov. Today, 16 (2011), pp. 1061-1068
9. Y.C. Kim, J.H. Park, M.R. Prausnitz, Microneedles for drug and vaccine delivery, Adv. Drug Deliver Rev., 64 (2012), pp. 1547-1568
10. K. Matsuo, S. Hirobe, N. Okada, S. Nakagawa, Frontiers of transcutaneous vaccination systems: novel technologies and devices for vaccine delivery, Vaccine, 31 (2013), pp. 2403-2415
11. N.G. Rouphael, M. Paine, R. Mosley, S. Henry, D.V. McAllister, H. Kalluri, W. Pewin, P.M. Frew, T. Yu, N.J. Thornburg, S. Kabbani, L. Lai, E.V. Vassilieva, I. Skountzou, R.W. Compans, M.J. Mulligan, M.R. Prausnitz, T.-M.S. Group, The safety, immunogenicity, and acceptability of inactivated influenza vaccine delivered by microneedle patch (TIV-MNP 2015): a randomised, partly blinded, placebo-controlled, phase 1 trial, Lancet, 390 (2017), pp. 649-658
12. C. Edens, M.L. Collins, J.L. Goodson, P.A. Rota, M.R. Prausnitz, A microneedle patch containing measles vaccine is immunogenic in non-human primates, Vaccine, 33 (2015), pp. 4712-4718
13. M. Leone, J. Monkare, J.A. Bouwstra, G. Kersten, Dissolving microneedle patches for dermal vaccination, Pharm. Res., 34 (2017), pp. 2223-2240
14. K. Matsuo, Y. Yokota, Y. Zhai, Y.S. Quan, F. Kamiyama, Y. Mukai, N. Okada, S. Nakagawa, A low-invasive and effective transcutaneous immunization system using a novel dissolving microneedle array for soluble and particulate antigens, J. Control Release, 161 (2012), pp. 10-17
15. Y. Qiu, L. Guo, S. Zhang, B. Xu, Y. Gao, Y. Hu, J. Hou, B. Bai, H. Shen, P. Mao, DNA-based vaccination against hepatitis B virus using dissolving microneedle arrays adjuvanted by cationic liposomes and CpG ODN, Drug Deliv. (2015), pp. 1-8
16. E.V. Vassilieva, H. Kalluri, D. McAllister, M.T. Taherbhai, E.S. Esser, W.P. Pewin, J.A. Pulit-Penaloza, M.R. Prausnitz, R.W. Compans, I. Skountzou, Improved immunogenicity of individual influenza vaccine components delivered with a novel dissolving microneedle patch stable at room temperature, Drug Deliv. Transl. Re, 5 (2015), pp. 360-371
17. E. Larraneta, R.E.M. Lutton, A.D. Woolfson, R.F. Donnelly, Microneedle arrays as transdermal and intradermal drug delivery systems: materials science, manufacture and commercial development, Mat. Sci. Eng. R, 104 (2016), pp. 1-32
18. J. Arya, M.R. Prausnitz, Microneedle patches for vaccination in developing countries, J. Control Release, 240 (2015), pp. 135-141

19. J. Monkare, M. Reza Nejadnik, K. Baccouche, S. Romeijn, W. Jiskoot, J.A. Bouwstra, IgG-loaded hyaluronan-based dissolving microneedles for intradermal protein delivery, J Control Release, 218 (2015), pp. 53-62
20. Y.K. Demir, Z. Akan, O. Kerimoglu, Characterization of polymeric microneedle arrays for transdermal drug delivery, PLoS ONE, 8 (2013), p. e77289
21. M.T. McCrudden, A.Z. Alkilani, C.M. McCrudden, E. McAlister, H.O. McCarthy, A.D. Woolfson, R.F. Donnelly, Design and physicochemical characterisation of novel dissolving polymeric microneedle arrays for transdermal delivery of high dose, low molecular weight drugs, J. Control Release, 180 (2014), pp. 71-80
22. S.D. Allison, A. Dong, J.F. Carpenter, Counteracting effects of thiocyanate and sucrose on chymotrypsinogen secondary structure and aggregation during freezing, drying, and rehydration, Biophys. J., 71 (1996), pp. 2022-2032
23. M. Katakam, L.N. Bell, A.K. Banga, Effect of surfactants on the physical stability of recombinant human growth hormone, J. Pharm. Sci., 84 (1995), pp. 713-716
24. S.J. Prestrelski, N. Tedeschi, T. Arakawa, J.F. Carpenter, Dehydration-induced conformational transitions in proteins and their inhibition by stabilizers, Biophys. J., 65 (1993), pp. 661-671
25. A.K.a.T. Takagi, Formation of Intermolecular β-sheet structure during heat denaturation of ovalbumin, J. Agric. Food. Chem., 36 (1988), pp. 1156-1159
26. W. Wang, Protein aggregation and its inhibition in biopharmaceutics, Int. J. Pharm., 289 (2005), pp. 1-30
27. W. Wang, S. Nema, D. Teagarden, Protein aggregation–pathways and influencing factors, Int. J. Pharm., 390 (2010), pp. 89-99
28. T. Arakawa, S.J. Prestrelski, W.C. Kenney, J.F. Carpenter, Factors affecting short-term and long-term stabilities of proteins, Adv. Drug Deliv. Rev., 46 (2001), pp. 307-326
29. N. Wilke, M.L. Reed, A. Morrissey, The evolution from convex corner undercut towards microneedle formation: theory and experimental verification, J. Micromech. Microeng., 16 (2006), pp. 808-814
30. K. van der Maaden, E. Sekerdag, W. Jiskoot, J. Bouwstra, Impact-insertion applicator improves reliability of skin penetration by solid microneedle arrays, Aaps J., 16 (2014), pp. 681-684
31. R. Blaine, Humidity Fixed Points, in: TA Instruments, 2004.
32. P. Schipper, K. van der Maaden, S. Romeijn, C. Oomens, G. Kersten, W. Jiskoot, J. Bouwstra, Repeated fractional intradermal dosing of an inactivated polio vaccine by a single hollow microneedle leads to superior immune responses, J. Control Release, 242 (2016), pp. 141-147
33. P. Schipper, K. van der Maaden, S. Romeijn, C. Oomens, G. Kersten, W. Jiskoot, J. Bouwstra, Determination of depth-dependent intradermal immunogenicity of adjuvanted inactivated polio vaccine delivered by microinjections via hollow microneedles, Pharm. Res., 33 (2016), pp. 2269-2279
34. K. van der Maaden, S.J. Trietsch, H. Kraan, E.M. Varypataki, S. Romeijn, R. Zwier, H.J. van der Linden, G. Kersten, T. Hankemeier, W. Jiskoot, J. Bouwstra, Novel hollow microneedle technology for depth-controlled microinjection-mediated dermal vaccination: a study with polio vaccine in rats, Pharm. Res., 31 (2014), pp. 1846-1854
35. L. Guo, J.M. Chen, Y.Q. Qiu, S.H. Zhang, B. Xu, Y.H. Gao, Enhanced transcutaneous immunization via dissolving microneedle array loaded with liposome encapsulated antigen and adjuvant, Int. J. Pharmaceut., 447 (2013), pp. 22-30
36. L.Y. Chu, S.O. Choi, M.R. Prausnitz, Fabrication of dissolving polymer microneedles for controlled drug encapsulation and delivery: Bubble and pedestal microneedle designs, J. Pharm. Sci., 99 (2010), pp. 4228-4238
37. M. Leone, B.H. van Oorschot, M.R. Nejadnik, A. Bocchino, M. Rosato, G. Kersten, C. O'Mahony, J. Bouwstra, K. van der Maaden, Universal applicator for digitally-controlled pressing force and impact velocity insertion of microneedles into skin, Pharmaceutics, 10 (2018)

38. K. Lee, C.Y. Lee, H. Jung, Dissolving microneedles for transdermal drug administration prepared by stepwise controlled drawing of maltose, Biomaterials, 32 (2011), pp. 3134-3140
39. K.A. Moga, L.R. Bickford, R.D. Geil, S.S. Dunn, A.A. Pandya, Y.P. Wang, J.H. Fain, C.F. Archuleta, A.T. O'Neill, J.M. DeSimone, Rapidly-dissolvable microneedle patches via a highly scalable and reproducible soft lithography approach, Adv. Mater., 25 (2013), pp. 5060-5066
40. Y. Hiraishi, T. Nakagawa, Y.S. Quan, F. Kamiyama, S. Hirobe, N. Okada, S. Nakagawa, Performance and characteristics evaluation of a sodium hyaluronate-based microneedle patch for a transcutaneous drug delivery system, Int. J. Pharm., 441 (2013), pp. 570-579
41. S. Liu, M.N. Jin, Y.S. Quan, F. Kamiyama, H. Katsumi, T. Sakane, A. Yamamoto, The development and characteristics of novel microneedle arrays fabricated from hyaluronic acid, and their application in the transdermal delivery of insulin, J. Control Release, 161 (2012), pp. 933-941
42. J.W. Lee, J.H. Park, M.R. Prausnitz, Dissolving microneedles for transdermal drug delivery, Biomaterials, 29 (2008), pp. 2113-2124
43. D. Krejcova, M. Pekarova, B. Safrankova, L. Kubala, The effect of different molecular weight hyaluronan on macrophage physiology, Neuro Endocrinol Lett, 30 (Suppl 1) (2009), pp. 106-111
44. S. Mizrahy, S.R. Raz, M. Hasgaard, H. Liu, N. Soffer-Tsur, K. Cohen, R. Dvash, D. Landsman-Milo, M.G. Bremer, S.M. Moghimi, D. Peer, Hyaluronan-coated nanoparticles: the influence of the molecular weight on CD44-hyaluronan interactions and on the immune response, J. Control Release, 156 (2011), pp. 231-238
45. C. Termeer, F. Benedix, J. Sleeman, C. Fieber, U. Voith, T. Ahrens, K. Miyake, M. Freudenberg, C. Galanos, J.C. Simon, Oligosaccharides of hyaluronan activate dendritic cells via toll-like receptor 4, J. Exp. Med., 195 (2002), pp. 99-111
46. C. Termeer, J.P. Sleeman, J.C. Simon, Hyaluronan–magic glue for the regulation of the immune response?, Trends Immunol., 24 (2003), pp. 112-114
47. C.C. Termeer, J. Hennies, U. Voith, T. Ahrens, J.M. Weiss, P. Prehm, J.C. Simon, Oligosaccharides of hyaluronan are potent activators of dendritic cells, J. Immunol., 165 (2000), pp. 1863-1870
48. M.J. Wang, J.S. Kuo, W.W. Lee, H.Y. Huang, W.F. Chen, S.Z. Lin, Translational event mediates differential production of tumor necrosis factor-alpha in hyaluronan-stimulated microglia and macrophages, J. Neurochem., 97 (2006), pp. 857-871
49. A.C.I. Depelsenaire, S.C. Meliga, C.L. McNeilly, F.E. Pearson, J.W. Coffey, O.L. Haigh, C.J. Flaim, I.H. Frazer, M.A.F. Kendall, Colocalization of cell death with antigen deposition in skin enhances vaccine immunogenicity, J. Invest. Dermatol., 134 (2014), pp. 2361-2370
50. G.S. Du, R.M. Hathout, M. Nasr, M.R. Nejadnik, J. Tu, R.I. Koning, A.J. Koster, B. Slutter, A. Kros, W. Jiskoot, J.A. Bouwstra, J. Monkare, Intradermal vaccination with hollow microneedles: a comparative study of various protein antigen and adjuvant encapsulated nanoparticles, J. Control Release, 266 (2017), pp. 109-118

SUPPLEMENTARY MATERIAL

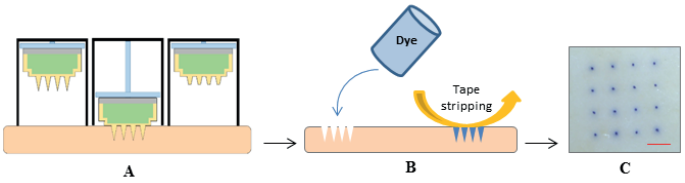

Supplementary Figure S1. Schematic representation of dissolving microneedle penetration and staining process. **(A)** The array is attached to the applicator piston. As the piston is lowered, the microneedles pierce the skin. After 18 seconds, the applicator piston is retrieved into its original position. **(B)** Pierced skin staining and SC removal by tape stripping. **(C)** Light microscope image (6.5x) of upper view of *ex vivo* human pierced skin. Each blue spot indicates effective microneedle penetration of the skin. Scale bar is 1 mm.

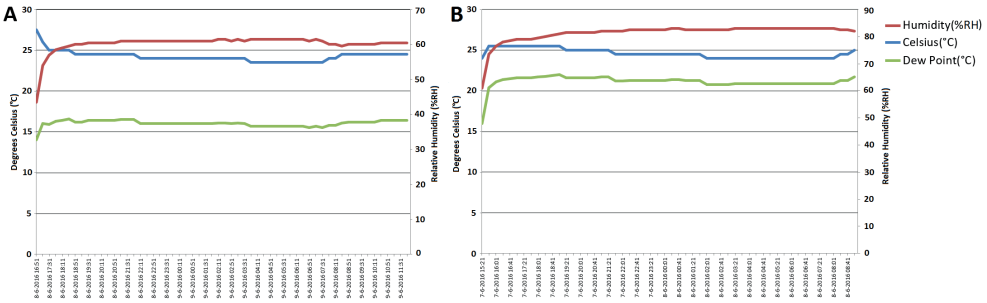

Supplementary Figure S2. Relative humidity values measured overnight every 20 min. Humidity graphs for sodium bromide **(A)** and potassium chloride **(B)**. The relative humidity, temperature and dew point of the solutions were measured by using a data logger (EL-USB-2-LCD+).

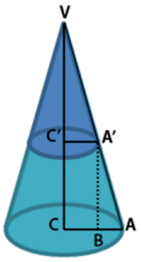

VC = H
VC' = h
CA = R
C'A' = r

ΔVC'A' and ΔVCA are similar

$$H : h = R : r \longrightarrow r = \frac{R \cdot h}{H} \qquad \text{(Equation 1)}$$

$$\textit{Dissolved cone volume} = \frac{1}{3} \cdot \pi \cdot r^2 \cdot h \qquad \text{(Equation 2)}$$

Supplementary Figure S3. Calculation of the dissolved MN percentage. To calculate the volume of the dissolved part of the needle the length of the dMN leftover was measured by using a microscope. Thus, the length of the MN dissolved part was calculated by subtracting the leftover from the original dMN length. Taking into account the original dMN length (H = 300 µm), the length of the dissolved part of the MN (h) and the radius of the base of the dMN (R = 100 µm), the top radius (r) can be calculated according to equation 1. Then, the volume of the dissolved part of the MN can be calculated (equation 2) and subsequently divided by the entire dMN volume to obtained the dissolved MN volume fraction.

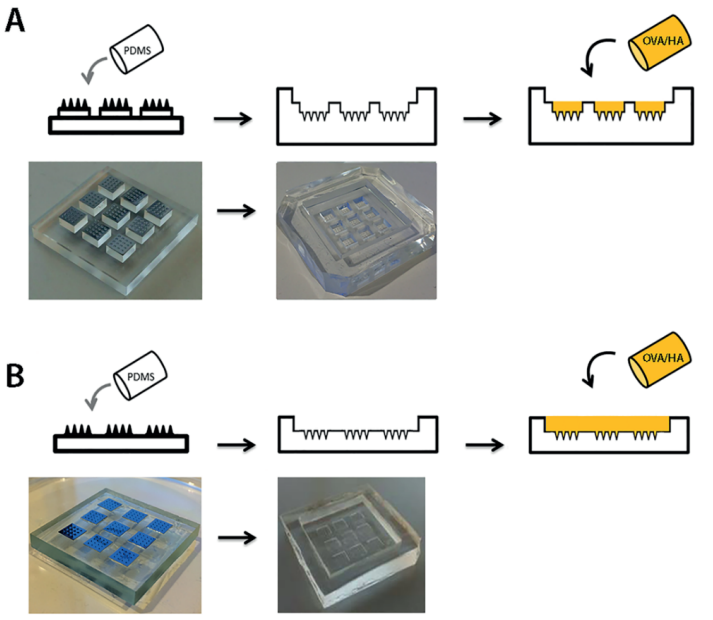

Supplementary Figure S4. Polydimethylsiloxane molds. **(A)** Single-array well design. On the left, the poly(methyl metacrylate) (PMMA) template used for the fabrication of the polydimethylsiloxane (PDMS) mold. The PMMA mold presents pedestals on which silicon arrays are fixed. On the right, the resulting PDMS mold presenting wells with microholes in which the OVA/HA solution can be poured. **(B)** Multi-arrays well design. On the left the PMMA template, without pedestals, producing a PDMS mold (right) with the arrays sharing the same fabrication space in which the OVA/HA solution can be poured.

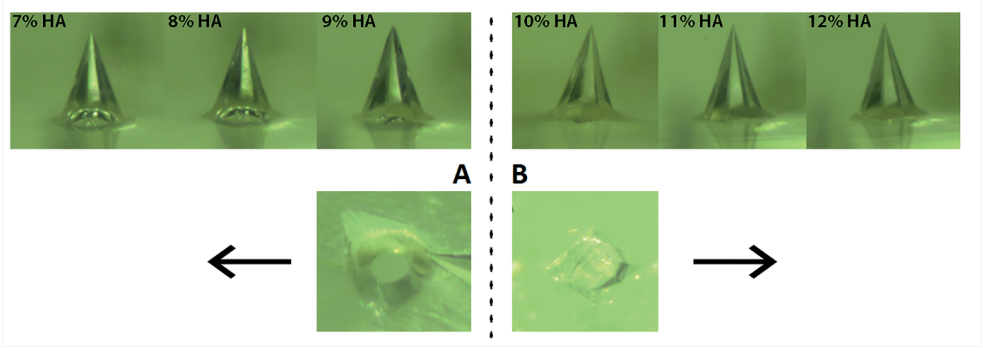

Supplementary Figure S5. Microscopic illustration of hyaluronan concentration optimization. Representative brightfield microscopy images (5x) of dMNs with increasing HA concentration (first row). In the second row, an upper view of a cut needle showing **(A)** a hole (observed for HA concentrations ≤ 9% (w/v)) and **(B)** without a hole (observed for HA concentrations > 9% (w/v)).

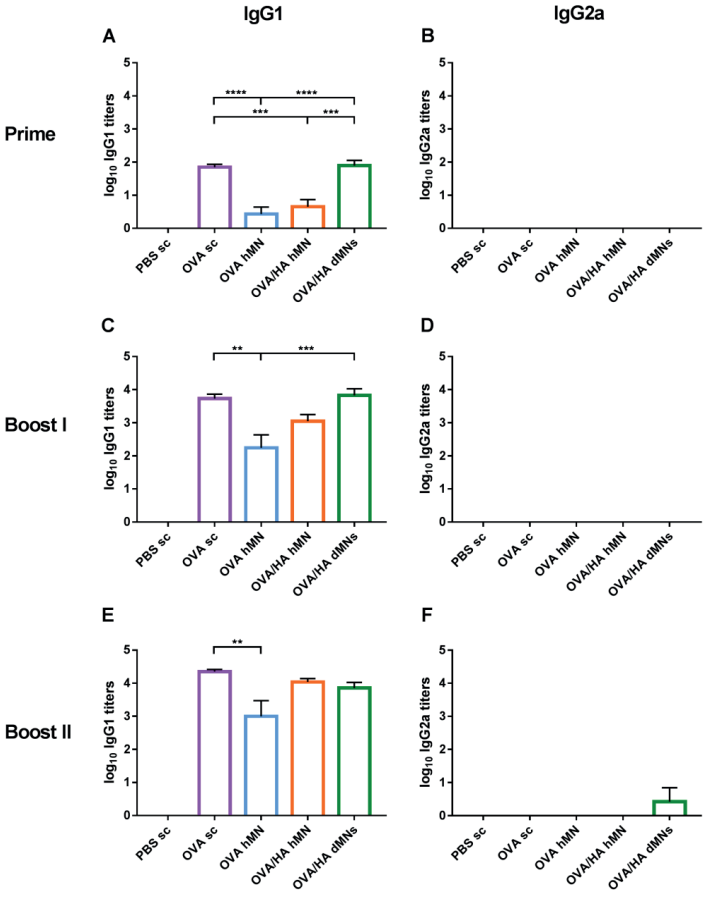

Supplementary Figure S6. OVA-specific IgG1 **(A, C, E)** and IgG2a **(B, D, F)** titers after prime **(A, B)**, 1st boost **(C, D)**, and 2nd boost **(E, F)** immunizations. Bars represent mean ± SEM, n = 8. **p < 0.01, ***p < 0.001, ****p<0.0001.